PROCEEDINGS OF SCIENCE

VHE Astrophysics: Theory vs Observations

Josep M. Paredes[*†]
Departament d'Astronomia i Meteorologia, Institut de Ciències del Cosmos, Universitat de Barcelona, IEEC-UB, Martí i Franquès 1, E-08028 Barcelona, Spain
E-mail: jmparedes@ub.edu

Pere Munar-Adrover
INAF-IAPS, Via Fosso del Cavaliere 100, 00133, Roma, Italy
E-mail: pere.munar@iaps.inaf.it

In the last two decades we have seen the dawn of the high energy gamma-ray astrophysics era. With the advent of the new Cherenkov telescopes and the space-based telescopes a new window to the extreme universe has been opened, bringing up an unprecedented sensitivity and resolution to study all kinds of very-high energy emitters, from AGNs to gamma-ray binaries. Here we describe some of the most important highlights in the very-high energy domain of the last fifteen years. Specifically, we overview the confirmation of galactic cosmic ray acceleration inside the supernova remnants IC 433 and W44, observations of the gamma-ray binaries PSR B1259−63 and LS 5039, the detection of rapid variability in blazars, and the detection of unprecedented flaring episodes of the Crab Nebula, among others. We also describe the theoretical challenges that such observational achievements have implied and how the new models may help to explain the data.

Frontier Research in Astrophysics,
26-31 May 2014
Mondello (Palermo), Italy

[*]Speaker.

[†]J.M.P. acknowledges support by DGI of the Spanish Ministerio de Economía y Competitividad (MINECO) under grant AYA2013-47447-C3-1-P and financial support from ICREA Academia.

PoS(FRAPWS2014)017

1. Introduction

High-energy astrophysics involves all the disciplines in the astrophysics field that are focused in the study of the processes involved in the emission of photons with energies at the X-ray domain and above. Above a certain energy in the X-rays, the emitted photons cannot be related to hot matter anymore. Thus, other mechanisms need to be invoked: non-thermal mechanisms. These processes are capable to inject large amounts of energy into a single particle. The physical scenarios where these phenomena take place are of various natures, usually related to strong shocks, powerful winds of massive stars, relativistic outflows ejected in the cores of active galactic nuclei (AGN), etc. In these scenarios, relativistic particles interact with the ambient matter, the magnetic fields and/or the photon fields to produce the detected gamma-ray emission.

The current generation of detectors have provided an unprecedented sensitivity and spatial resolution to study the extreme universe. In the high-energy (HE) gamma-ray domain, the space missions such as *AGILE* and *Fermi*/LAT provide the scientific community with unvaluable data from processes with energies ranging from 0.3 to 300 GeV. They are continuously studying AGN, gamma-ray bursts, binary systems, etc., with excellent results. For processes producing even higher energy radiation, the context of this review, we take advantage from the Atmospheric Imaging Cherenkov Telescopes (IACTs), which with their big collecting areas are capable to detect the few >100 GeV photons that make their trip to the Earth through the air showers developed when the VHE photons interact with the atmosphere. The current VHE source catalog comprises 161 sources (see `http://tevcat.uchicago.edu/`), from AGN to gamma-ray binaries.

In the next sections we will revisit the latest highlights in the field of VHE astrophysics.

2. Extragalactic sources

2.1 Blazars

Within the blazar AGN subtype, there are the high-peaked BL Lac (HBL) objects, which are characterized by showing a spectral energy distribution (SED) in which both maxima (at X-rays and HE/VHE gamma-rays, respectively) occur at relatively high frequency. The detection of gamma rays from blazars implies that the environment is optically thin in the emitting region, which requires the presence of relativistic beaming to decrease the intrinsic energy density of the soft target photons inside the source.

To explain the detected gamma-ray emission from blazars there are two main group of models: leptonic and hadronic models, respectively. In the case of leptonic models, the same relativistic electrons responsible for the broad-band emission from radio to X-rays are responsible for the gamma-ray emission, through Compton upscattering of the synchrotron photons that were created by their own parent electrons; this is the so-called synchrotron self-Compton process (SSC) (Marscher & Gear 1985; Maraschi et al. 1992). In other leptonic models, electrons scatter external photons originated outside the jet (e.g. from the accretion disk). The lack of strong emission lines in BL Lac objects indicates a minor role of ambient photons and hence supports the SSC mechanism. The hadronic models explain the detected gamma-ray emission by means of hadronic interactions of the highly relativistic baryon flow with the ambient medium, or by the interaccion of ultra-high

energetic protons with synchrotron photons produced by electrons (Mannheim & Biermann 1992), with the jet magnetic field (Aharonian 2000) or with both (Atoyan & Dermer 2003).

2.1.1 Markarian 501

In 2007 the MAGIC Collaboration reported on the detection of rapid flux variability in the Blazar Markarian 501 (Mrk 501) (Albert et al. 2007a). MAGIC observed this source for six weeks in summer 2005. In two nights Mrk 501 exhibited short flares with a variability in timescales of ~ 2 minutes in the 0.15−10 TeV energy band, and also a very short flux-doubling time $\lesssim 3$ minutes. This facts can give important information about the acceleration processes occuring in blazars.

During these two nights, the behaviour of Mrk 501 was slightly different during the flares: in the first night the flare was visible in the 0.25−1.2 TeV energy range, while in the second night it was visible at all the energies (from 0.12 to >1.2 TeV). The analysis of the data revealed also a delay in the arrival of photons with different energies: at a zero-delay probability of $p = 0.026$, a marginal time delay of $\tau_1 = (0.030 \pm 0.012)$ s GeV^{-1} towards higher energies was found using two independent analyses. One of the explanations for this delay is the energy dependent speed of light in the vacuum, as predicted in some models of quantum gravity where Lorentz invariance violation is a manifestation of the foamy structure of space-time at short distances.

2.1.2 PKS 2155-304

On July 2006 the H.E.S.S. Cherenkov telescope observed the high-frequency peaked BL Lac object PKS 2155-304 and detected several rapid flaring events with a flux more than 10 times the average flux usualy measured in this object. The H.E.S.S. Collaboration reported on an extreme gamma-ray outburst in the early hours of 2006 July 28 with a flux of $F(E > 200 \text{ GeV}) = (1.72 \pm 0.05_{\text{stat}} \pm 0.34_{\text{sys}}) \times 10^{-9}$ cm^{-2} s^{-1}, corresponding to ~ 7 times the Crab Nebula flux above 200 GeV (Aharonian et al. 2007a). Superluminal expansions observed with VLBI (Piner & Edwards 2004) provided evidence for moderate Doppler boosting in PKS 2155-304. The size of the emitting region can be obtained from its relation with the flux rise time and the Doppler factor δ by $R \leq ct_{\text{var}}\delta/(1+z)$. For a value of $t_{\text{var}} = 173 \pm 28$ s the size of the emitting region is constrained to $R\delta^{-1} \leq 4.65 \times 10^{12}$ cm ≤ 0.31 AU, which is a very compact region. The rapid variability in PKS 2155-304 implies also that the bulk emitting particles must be moving with large Lorentz factors to overcome the pair-opacity and relax the size constraint. Assuming that the variable emission is produced very close to the super-massive black hole (SMBH) the mass can be constrained to $M_{\text{SMBH}} \sim 10^7$ $M_\odot$. The apparent periodicity of the subflares observed could provide a measure of the angular momentum of the SMBH (Neronov et al. 2008).

The SED of PKS 2155-304 during the 2008 observations was computed in order to fit the lower energy observations and the high-energy component was fitted afterwards by adjusting other model parameters, such as the emitting region size in the comoving reference frame, the Doppler factor and the magnetic field. This model, although simple, allows one to describe the joint *Fermi*-H.E.S.S. time averaged spectra with a SSC emission model. The variability patterns in the optical, X-ray, HE, and VHE bands suggest a much more complex situation. In the absence of spectral variability, the mechanisms that would produce the observed flux variability in the VHE band are rather constrained. Increases in flux could be driven by injection of particles with a constant spectral shape, and decreases in flux could be caused by particle escape from the emitting region

or by expansion (adiabatic) losses, assuming that these two processes can operate independently of particle energy. However, since the electrons that produce the VHE emission must be in the weak radiative cooling regime, a more natural mechanism for the flux variability would be changes in the seed photon density. Comparing the daily flux values in the optical and the VHE bands, they found indications of fairly strong correlations that suggest that the optical emission provides the target photons for the IC emission. In the B, V, and R bands, the correlations with the H.E.S.S. fluxes have Pearson's r values in the range 0.77−0.86 with uncertainties ≤ 0.09. These results provide the first quantitative evidence of correlated variability between the optical and VHE bands on these timescales for an HBL. Confirmation of this behavior, not only from this source but also from other VHE emitting blazars in a low state, would provide important constraints on emission models for these objects.

2.2 Radio Galaxies

Blazars are not the only extragalactic objects emitting VHE gamma rays. Radio galaxies display powerfull radio jets that are not pointed towards our line of sight and thanks to their orientation and proximity we can study their jet structure in detail.

So far, four radio galaxies have been detected by the current generation of IACTs at VHE gamma-ray energies: Cen-A, M 87, NGC 1275 and IC 310. The M87 radio galaxy has long been known as a VHE emitter (Aharonian et al. 2006b). The H.E.S.S., MAGIC and VERITAS Collaborations carried out a joint monitoring campaign in order to study its variability timescales and the location of the VHE emitter. This resulted in $\sim$ 120 h of observations in 2008 (Acciari et al. 2009a), which revealed the presence of periods of strong VHE gamma-ray flares followed by an important increase of the radio flux from the galactic nucleus. MAGIC measured in 2008 the spectrum of M87 below 250 GeV (Albert et al. 2008), describing it with a powerlaw with spectral index $\Gamma = 2.30 \pm 0.11_{\rm stat} \pm 0.20_{\rm sys}$. A variability in a night-to-night basis for energies above 350 GeV was reported by MAGIC, while no variability was found below this energy. This allows for constraining the emitting region size to $R \leq \Delta t c \delta = 2.6 \times 10^{15}$ cm and suggests the core of M87 jet as the TeV emitter. During the MAGIC observations the knot HST-1 displayed a minimum in its ever observed X-ray luminosity, whereas the core displayed a maximum, thus supporting it to be the origin of the VHE emission.

3. Galactic sources

3.1 Galactic Center

The possibility to detect dark matter that annihilates into VHE gamma rays has brought interest in observing the Galactic Center (GC) with the current Cherenkov telescopes. H.E.S.S. and MAGIC have observed the GC measuring a steady flux at VHE which can be fitted by a powerlaw with photon index $\Gamma \sim 2.2$, up to energies of $\sim$ 20 TeV with no indication of a cut-off (Aharonian et al. 2004; Albert et al. 2006a). H.E.S.S. reported in 2009 the existence of a cut-off in the powerlaw spectrum with a photon index $\Gamma = 2.10 \pm 0.04_{\rm stat} \pm 0.10_{\rm sys}$ and a cut-off energy at $E_{\rm co} = 15.7 \pm 3.4_{\rm stat} \pm 2.5_{\rm sys}$ TeV (Aharonian et al. 2009). The curvature of the energy spectrum is likely to be intrinsic to the emitting source instead of being due to effects of interstellar absorption.

There is no evidence of variability in the VHE data, indicating that the emission regions must differ from the invoked for the variable IR and X-ray emission.

In the recent years the gamma-ray emission from the GC has been interpreted as the product of dark matter annihilation, producing leptons with energies between 7 and 12 GeV, which in turn would produce a haze of synchrotron emission, very similar to the one observed by WMAP (Hooper & Linden 2011). Crocker et al. (2011) (see also references therein) studied the inner region of the Galaxy showing that the power injected by supernovae exploding every few thousand years accelerate the GC CR population and produce TeV gamma-rays. Other works, such as Bednarek & Sobczak (2014), suggest that the GeV-TeV emission observed from the GC is a cumulative effect of the emission from several globular clusters captured by the GC black hole. There is still no clear evidence of any of the two proposed scenarios for the GC emission (Mirabal 2013).

It was expected that the passage of a dust cloud near SgrA* (Gillessen et al. 2012; Eckart et al. 2013) in September 2013 would produce flare events. Although some scenarios for this encounter predicted variable VHE emission (Ballantyne et al. 2011), no evidence of such activity has been observed until now.

3.2 Supernova Remnants

Galactic cosmic rays (CR) have been suspected to be produced in supernova remnants (SNR) for long time. However, to prove the acceleration of CR in SNR shells we need to explain unambiguously the SNR SED with a hadronic model, which still is difficult nowadays. In most cases, the SED can be explained by leptonic or hadronic models, as for instance in the case of RX J1713.7−3946 (Aharonian et al. 2006a). In this case, the favoured model depends on the value of the magnetic field (B $\sim$ 10μG for leptonic model and B $\sim$ 100μG for a hadronic model). The morphology of the VHE emission ressembles very well the X-ray emission and presents a photon index of ∼2.2. It is remarkable that the emission extends well above 30 TeV and there is evidence of emission above 100 TeV, thus proving the acceleration of particles up to energies $\sim 10^{15}$ eV, very close to the value for the knee in the CR spectrum.

The hadronic interpretation is often favoured in SNRs. The X-ray spectrum is well explained by synchrotron emission from relativistic electrons accelerated in the forward shock of the remnant interacting with strong magnetic fields, of the order of 100μG, a value much larger than that typically observed in the interstellar medium. The high magnetic field disfavours the IC interpretation of the VHE emission, thus leaving room for a hadronic origin. However, the hadronic interpretation requires a higher density which is in contradiction with the absence of thermal X-rays arising from the remnant (Aharonian et al. 2006a, 2007b). The spectrum collected with the *Fermi*/LAT and H.E.S.S. can be fitted with both models.

3.2.1 Tycho SNR

In 2011 the VERITAS Collaboration reported the detection of VHE gamma rays coming from the Tycho SNR (G120.1+1.4) (Acciari et al. 2011). This is a young (438 year) SNR which has been extensively studied at many wavelengths. Non-thermal X-ray emisson has been detected mainly from the rim of the remnant (Hwang et al. 2002; Katsuda et al. 2010) and filamentary X-ray emission in this region have been interpreted as evidence for electron acceleration (Hwang et al. 2002; Warren et al. 2005).

At VHE, the integral flux detected is very faint, being at the level of 0.9% of the Crab Nebula flux above 1 TeV. The spectrum of this source was fitted with a powerlaw model with $\Gamma = 1.95 \pm 0.51_{\rm stat} \pm 0.30_{\rm sys}$ and theoretical models allow for an interpretation with both leptonic and mixed (hadronic plus leptonic) origin of the emission. The lowest magnetic field allowed in these models is $\sim 80\mu$G, which may be interpreted as evidence for magnetic field amplification within the SNR. The emission at VHE is displaced towards the north-east of the remnant. This is interpreted as the result of the interaction of the particles accelerated in the shock of the SNR with a nearby high-density molecular cloud.

3.2.2 W51

In a class of more evolved SNR systems, we find the W51 complex. This is a SNR that seems to be interacting with a nearby molecular cloud in W51B region. Aleksić et al. (2012a) detected VHE gamma-ray emission from this SNR with clear extended morphology, and measured its flux in the 75 GeV−4 TeV energy range. The spectrum of the source is fitted with a powerlaw with photon index $\Gamma = 2.6$ and is compatible with the measurement with the *Fermi*/LAT between 2 and 40 GeV. The spectrum measured with MAGIC allows for the first time the determination of the slope of the parent particle distribution above the spectral break measured by *Fermi*/LAT above a few GeV.

The emission detected by MAGIC is spatially coincident with the previous reported sources by H.E.S.S. and *Fermi*/LAT and moreover, it has been constrained to the region where W51C (the SNR) interacts with the W51B molecular cloud, and in particular, to the region where shocked gas is observed. This is a clear evidence for an origin of the VHE emission in the interaction region between the SNR and the cloud. The emission of this remnant can only be modeled within a hadronic scenario, being neutral pion decay the main source of VHE gamma rays. This implies a parent proton population accelerated up to more than 100 TeV. The morphology of the source cannot be explained by CRs diffusing from the SNR to the cloud. This emission can be interpreted as produced in the CRs acceleration site. This implies reacceleration of CRs present in the shocked cloud region.

3.2.3 IC 433 and W44

The clear detection of the pion decay signature in the VHE emission of SNRs has been difficult since the electrons are also capable to produce VHE gamma rays via relativistic Bremsstrahlung and IC emission. Ackermann et al. (2013) have reported the detection of such a signature recently in two SNRs, IC 443 and W44, using the *Fermi*/LAT data. When the relativistic protons are accelerated in the SNR shock region they interact with atomic nuclei, causing their decay into π^0 mesons which, in turn, will produce two gamma-ray photons when they decay. These photons have an energy of 67.5 MeV in the rest frame of the neutral pion. The spectrum of gamma rays will be then symmetric about 67.5 MeV in a log-log representation. The $E^2F(E)$ representation of the π^0-decay rises quite steep below $\sim$ 200 MeV and aproximately traces the energy distribution of the parent proton population at energies above a few GeV. In between there is a characteristic spectral feature known as the pion-decay bump, which uniquely identifies the π^0-decay and thus the relativistic protons, allowing for a measurement of the source spectrum of CRs.

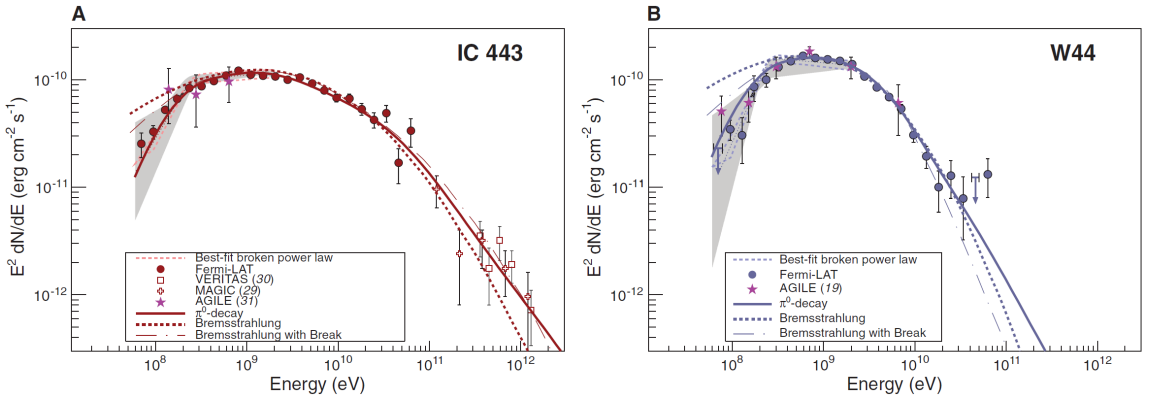

Figure 1: Gamma-ray spectra of IC 443 and W44 from Ackermann et al. (2013). Solid lines denote the bestfit pion-decay gamma-ray spectra, dashed lines denote the best-fit Bremsstrahlung spectra, and dash-dotted lines denote the best-fit bremsstrahlung spectra when including an ad hoc low-energy break at 300 MeV c^{-1} in the electron spectrum. These fits were done to the *Fermi*/LAT data alone (not taking the TeV data points into account).

In the case of IC 443 and W44, both source spectra below 200 MeV rise steeply, clearly exhibiting a break at $\sim$ 200 MeV. A fit with an smoothly broken powerlaw with two indexes is, in both cases, statisticaly better than a single powerlaw. A π^0-decay spectral model yields a very good match to the data in Ackermann et al. (2013). In this case, the measured gamma-ray spectra, in particular the low-energy parts, matched the π^0-decay model (see Figure 1). However, the spectral parameters obtained with this model are in contradiction with what one could expect if the interaction between a cosmic-ray precursor and adjacent molecular clouds were responsible for the bulk of the observed GeV gamma rays: the observed spectrum should be much harder, in contradiction with what is observed with *Fermi*/LAT data. π^0-decay is probably produced by interactions between the cloud that has been crushed by the SNR and relativistic protons. Filamentary synchrotron structures seen in high-resolution radio images support this theory. Since the cloud where this emission is produced is geometrically thin, particles are expected to be able to escape the region, which may explain the break observed in the fitted spectra. The measurement of the break and the data down to 60 MeV from *Fermi*/LAT provide evidence for the first time for the acceleration of protons in SNRs.

3.3 Pulsar Wind Nebulae

Pulsar wind nebulae (PWN) form when the relativistic electron/positron wind of a young pulsar interacts with the ambient magnetic and photon fields, producing synchrotron and IC emission, respectively. Hence, the HE and VHE emission of these objects is most probably produced by leptonic mechanisms, while hadronic processes seem to be disfavoured. This family of objects represents the major Galactic TeV source population, with more than 15 PWN already detected by H.E.S.S., most of them showing an extended morphology at TeV energies. The electrons/positrons that produce the detected IC emission must have been accelerated up to energies of $\sim$ 100 TeV.

3.3.1 MSH 15−52

Among many cases, there is the source MSH 15−52, which has been reported to be extended at GeV energies by the *Fermi* Collaboration (Abdo et al. 2010). This is a PWN containing a young rotating pulsar with a period of 150 ms. It has been observed at all posible wavelengths, from radio to gamma rays. The inferred surface magnetic field of this pulsar is 1.5×10^{13} G, derived under the assumption of a dipolar magnetic field, and the spin-down power is 1.8×10^{37} erg s^{-1}. This pulsar shows an extended morphology at energies above 10 GeV as seen by the *Fermi*/LAT which is spatially coincident with the TeV emission reported by the H.E.S.S. Collaboration (Aharonian et al. 2005b) and also with the location of the pulsar PSR B1509−58. Abdo et al. (2010) also report the detection of pulsed emission from this source below 1 GeV using the 1-year data set of *Fermi*/LAT. The broadband spectrum of this source can be explained by a leptonic model introducing synchrotron and IC emission, assuming a broken powerlaw spectrum for electrons. Multi-wavelength observations provide indications of a spectral break which is thought to be caused by an intrinsic break of electrons injected from the pulsar wind.

3.3.2 HESS J1825−137

Another interesting PWN is HESS J1825−137 which was discovered as an extended TeV source by the H.E.S.S. Collaboration (Aharonian et al. 2005d, 2006c) during the galactic plane scan. It is associated to the energetic pulsar PSR J1826−1334, which has a spin-down luminosity of 3×10^{36} erg s^{-1} and is located at a distance of 3.9 ± 0.4 kpc (Cordes & Lazio 2002). In X-rays there is a compact central source associated to the pulsar and a surrounding diffuse X-ray emission region, interpreted as synchrotron emission due to the efects of the relativistic pulsar wind, forming the PWN (Gaensler et al. 2003). The X-ray diffuse emission is assymmetrical in shape. Gaensler et al. (2003) interpret that this assymmetry is produced by the expansion of the PWN colliding with dense material in the north side of the pulsar, shifting the whole emission to the south. This source provided also the first evidence for an energy-dependend morphology at TeV gamma rays, showing a softening of the VHE spectrum of the source with the distance to the central emitter. This is interpreted as synchrotron and IC cooling of electrons within the nebula. The X-ray detected emission is smaller in size than the VHE emission, due to the fact that X-ray emitting particles cool faster than TeV emitting ones.

3.3.3 Crab Nebula

One of the most intriguing sources is the PWN known as the Crab Nebula. This is the relic of a supernova explosion that occured in 1054 A.D. This source has been used as the standard candle for gamma-ray astrophysics given its steady behaviour, until it showed a clearly variable behaviour in 2011. The Crab Nebula is powered by the powerful Crab pulsar, with spin-down luminosity of 5×10^{38} erg s^{-1} and a rotation period of 33 ms (Rees & Gunn 1974). The Crab Nebula X-ray continuum and gamma rays up to 100 MeV energies are modeled by means of synchrotron radiation, and emission from GeV to TeV energies as IC radiation from accelerated electrons scattering the cosmic microwave background and nebular photons (Tavani et al. 2011 and references therein).

In September 2010 an unexpected gamma-ray flare from the direction of the Crab Nebula was detected by *AGILE* at energies above 100 MeV (Tavani et al. 2011). The detected flux was

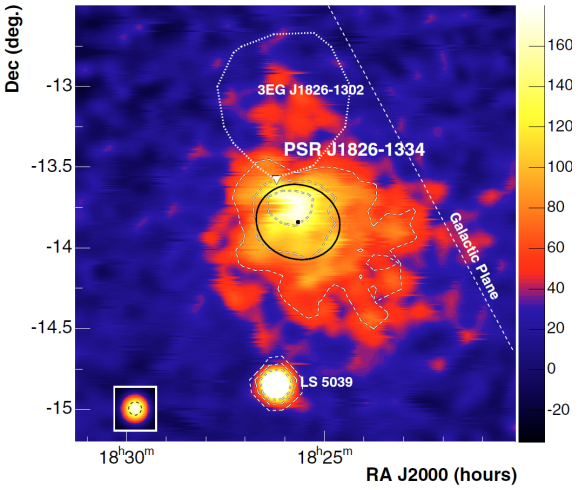

Figure 2: Excess map in the $2.7^\circ \times 2.7^\circ$ field of view surrounding HESS J1825−137 (Aharonian et al. 2006c). The inset in the bottom left corner shows the PSF of the dataset. The dashed black and white contours are linearly spaced and denote the 5σ, 10σ and 15σ significance levels (the 5σ contour being the outermost one), determined with a $\theta = 0.1^\circ$ radius cut. The best fit position of HESS J1825−137 is marked with a black square, and the best extension and position angle by a black ellipse (see Aharonian et al. (2006c)). The dotted white contour shows the 95% positional confidence contour of the unidentified *EGRET* source 3EG J1826−1302. The position of the pulsar PSR J1826−1334 is marked by a white triangle.

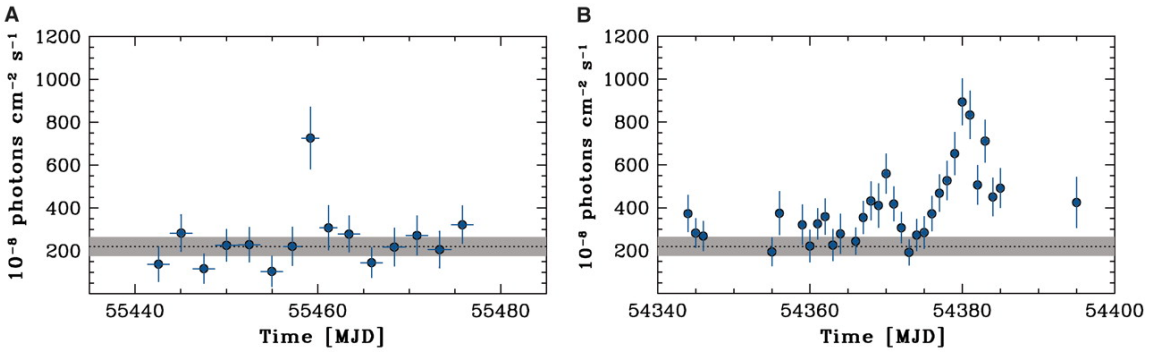

Figure 3: Crab Nebula light curves of the total flux detected by *AGILE* in the energy range of 100 MeV to 5 GeV during the gamma-ray flaring periods in 2007 and 2010 (units of 10^{-8} cm^{-2} s^{-1}). (A) The spinning *AGILE* photon flux light curve during the period 2 September to 8 October 2010. Time bins are 2.5 days except near the flare peak (2-day binning). Errors are 1 SD, and time is given in Modified Julian Day (MJD). The dotted line and gray band show the average Crab flux and the 3 SD uncertainty range. (B) The AGILE light curve during the period 27 September to 12 October 2007 (1-day binning) with the satellite in pointing mode. Errors are 1 SD. Time is given in MJD. The dotted line and gray band show the average Crab flux and the 3 SD uncertainty range. Image from Tavani et al. (2011).

$F = (7.2 \pm 1.4) \times 10^{-6}$ cm^{-2} s^{-1} with a photon index $\alpha = 2.03 \pm 0.18$, for a 4.8 standard deviations (SD) detection above the average flux. In the subsequent 2-3 days, the source decayed to normal average values (see Figure 3). This flare was independently confirmed by the *Fermi*/LAT (Abdo et al. 2011a).

In 2007 *AGILE* detected another gamma-ray flare from the Crab Nebula, lasting for two weeks, with a peak flux of $F = (8.9 \pm 1.1) \times 10^{-6}$ cm^{-2} s^{-1} with a photon index $\alpha = 2.05 \pm 0.13$, for a 6.2 SD detection above the average flux (Pittori et al. 2009).

In both 2007 and 2010 events, the flux obtained from the pulsar remained within its average values at all observed wavelengths. Tavani et al. (2011) atributed the flares to unpulsed relativistic shock emission originated in the nebula. The short duration of the detected flares implies that the gamma rays were emitted via synchrotron emission from electrons with energies above 1 PeV in a region smaller than 1.4×10^{-2} pc (Abdo et al. 2011a). These are the highest-energy particles that can be associated to a discrete astronomical source, and they pose challenges to particle acceleration theory.

Bednarek & Idec (2011) propose that the variable gamma-ray emission observed during the 2010 events in the Crab Nebula is caused by an emission region behind the shock in the pulsar wind, which is moving mildly relativistically to the observer. In this region, electrons can be accelerated at different maximum energies as a result of the reconnection of the magnetic field compressed by the decelerating pulsar wind (Cerutti et al. 2012; Lyutikov 2014; Bühler & Blandford 2014, and references therein). These electrons produce synchrotron emission in the MeV-GeV range, and IC gamma rays above 1 TeV by scattering of the CMB photons and the low-energy synchrotron radiation.

3.4 Pulsars

In the case of the emission at HE and VHE from pulsars, it is generally accepted that the primary radiation mechanism in pulsar magnetospheres is synchrotron-curvature radiation. This mechanism takes place as electrons move along the magnetic field lines in the extremely strong field of the pulsar. Other emission mechanisms include ordinary synchrotron and IC processes.

One of the best studied VHE sources is the Crab Nebula and its pulsar. The Crab pulsar has been observed at all possible wavelengths. In the last years, the Crab pulsar was detected at VHE energies above ~25 GeV by the MAGIC Telescope (Aliu et al. 2008). It was seen at that time that the pulsed emission at VHE was in phase with the detected HE emission seen with *EGRET* and also in the optical band observed with the MAGIC central pixel. The phase averaged spectrum shows an spectral cut-off at relatively high energies, telling that the emission seems to be produced in a region far from the pulsar magnetosphere. These results excluded the polar-cap model and challenge the slot-gap model for the Crab pulsar.

Moreover, in subsequent observations with Cherenkov telescopes, it was seen that the pulsed emission of the Crab pulsar extended up to even higher energies. It was first announced the detection by VERITAS of pulsed emission from the Crab pulsar above 250 GeV (VERITAS Collaboration et al. 2011) and afterwards by MAGIC for energies above 400 GeV (Aleksić et al. 2012c), as can be seen in Figure 4. These detections at such high energies challenged all available models. The interpretation of these detections is that the emission comes from an additional VHE component produced by the IC scattering of secondary and tertiary electrons/positrons on IR and UV photons. Aharonian et al. (2012) worked in the explanation of the VHE component of the Crab pulsar. In their interpretation the VHE data is explained by IC emission via the scattering of magnetospheric X-rays. For this to work, they introduce a cold ultrarelativistic wind dominated by kinetic energy. The conversion of the Poynting flux into kinetic energy should occur abruptly in a

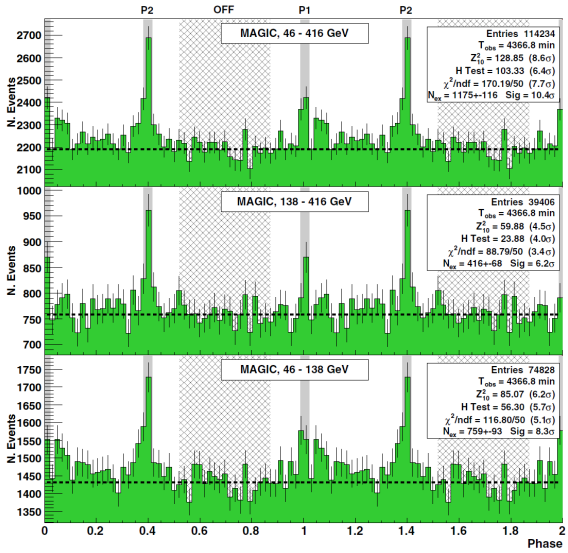

Figure 4: MAGIC folded light curves of the Crab pulsar for the total range in estimated energy and for two separate sub-bins. The shaded areas are the on-phase regions P1M and P2M, and the light shaded area is the off-region [0.52−0.87]. The dashed line is the constant background level calculated from that off-region. Image from Aleksić et al. (2012).

narrow cylindrical zone with a radius between 20 and 50 light-cylinder radii, and should accelerate the electrons/positrons of the wind up to Lorentz factors above 5×10^6. This conclusion does not agree with those of alternative models, for example the so-called reconnection models of pulsar wind nebulae (Coroniti 1990; Lyubarsky & Kirk 2001) based on the assumption that the transformation of the Poynting flux to kinetic energy of bulk motion is a slow process that takes place over the entire region of the unshocked wind.

3.5 Binary systems

With the advent of a new generation of space- and ground-based telescopes in the last years, a new family of gamma-ray emitting systems has arisen: the gamma-ray binaries. Most of the known systems belong to the high-mass X-ray binary (HMXB) class. The detection of HMXBs at GeV and/or TeV energies has been the focus of extensive studies in the past few decades, but only a few systems have been confirmed as gamma-ray emitters, including PSR B1259−63 (Aharonian et al. 2005c), LS 5039 (Aharonian et al. 2006d), LS I +61 303 (Albert et al. 2006b, 2009; Anderhub et al. 2009; Aleksić et al. 2012d), HESS J0632+057 (Acciari et al. 2009b; Aleksić et al. 2012b; Aliu et al. 2014) and Cygnus X-3 (Fermi LAT Collaboration et al. 2009; Tavani et al. 2009). Another gamma-ray binary system, 1FGL J1018.6−5856 (Fermi LAT Collaboration et al. 2012; H. E. S. S. Collaboration et al. 2012) has also been detected at TeV energies, although its emission has not been regularly detected.

In order to explain the broadband emission of all these systems, two main paradigms have appeared along the years (Maraschi & Treves 1981, Bosch-Ramon & Khangulyan 2009, Dubus 2013): the microquasar and the binary-pulsar scenarios. In the first one, the compact object is accreting material from the companion star through Roche-lobe overflow via an accretion disk.

Whilst this accretion takes place, two jets are formed perpendicular to the accretion disk. These jets carry on relativistic particles that would be behind the detected non-thermal emission. In the binary-pulsar scenario the non-thermal emission arises from the interaction of the relativistic wind of a young non-accreting pulsar with the wind of the massive companion star.

In the near future, the new generation of Cherenkov telescopes, with CTA as the principal observatory, will help us to unveil more characteristics of the physics underlying these extreme accelerators (Paredes et al. 2013).

3.5.1 Microquasars

Cygnus X-1 is a microquasar which was observed by MAGIC in 2006. From these observations Albert et al. (2007b) reported a 4.1σ hint of detection of this system, which occurred coinciding with an X-ray flare seen by *RXTE*, *Swift* and *INTEGRAL*. The *AGILE* collaboration also reported the detection of flaring activity from this HMXB (Bulgarelli et al. 2010; Sabatini et al. 2010). The hint of emission seen by MAGIC is interpreted (Romero et al. 2010) as a jet-cloud interaction (Araudo et al. 2009). Protons from the jet interact with ions in a cloud of clumpy wind from the companion star, producing inelastic *pp*-collisions and pion decay, which produces a flare in TeV gamma rays.

Cygnus X-3 harbours a Wolf-Rayet star as a companion and an accreting compact object. The accretion launches two jets and it is now thought that one of the jets must be slightly inclined towards the line of sight. The GeV emission would be produced when relativistic electrons in the jet up-scatter photons from the companion. The orbital variability is naturally explained by the inclination of the jet and that the emitting electrons are located at 1–10 times the orbital separation of the binary system (Dubus et al. 2010). At this distance, a recollimation shock could be formed and the electrons accelerated, and thus, these electrons would be capable to produce IC scattering on the donor star photons.

Very recently, a new member of the microquasar family has been reported: MWC 656 (Casares et al. 2014). This system, located at 2.6±0.6 kpc, is composed by a Be star and a 3.8−6.9 $M_\odot$ black hole (BH) and is the only system of this kind detected so far. It is also a gamma-ray binary candidate since 2010 when *AGILE* reported a flare coming from a region containing MWC 656. It was later confirmed as a binary system with a period of 60.37 days (Williams et al. 2010; Casares et al. 2012). In a subsequent work, Casares et al. (2014) presented new data and a double-line solution to the radial velocity curves of the two binary components, allowing them to obtain physical parameters: eccentricity of 0.10±0.04, periastron orbital phase $\phi_{\rm per} = 0.01 \pm 0.10$, and mass ratio $M_2/M_1 = 0.41 \pm 0.07$. They also updated the spectral classification of the Be star to B1.5–B2 III, which implies a Be mass in the range 10–16 $M_\odot$ and, therefore, a BH companion of 3.8–6.9 $M_\odot$. This makes MWC 656 the first Be binary with a BH companion. Munar-Adrover et al. (2014) established MWC 656 as a HMXB through X-ray observations with XMM-Newton. These authors reported the discovery of the X-ray counterpart of this binary system at orbital phase 0.08. The X-ray spectrum of MWC 656 is fitted with a black body plus a power-law, with the non-thermal component dominating above ∼0.8 keV. The non-thermal X-ray luminosity of MWC 656 is $L_{\rm nt}(0.3{-}5.5\ {\rm keV}) = \left(1.6^{+1.0}_{-0.9}\right) \times 10^{31}\ {\rm erg\ s^{-1}} \equiv (3.1 \pm 2.3) \times 10^{-8} L_{\rm Edd}$ (Munar-Adrover et al. 2014) for the estimated BH mass range 3.8–6.9 $M_\odot$ (Casares et al. 2014). This non-thermal emission is interpreted as X-rays arising from close to the BH. The X-ray flux of MWC 656 is comparable to

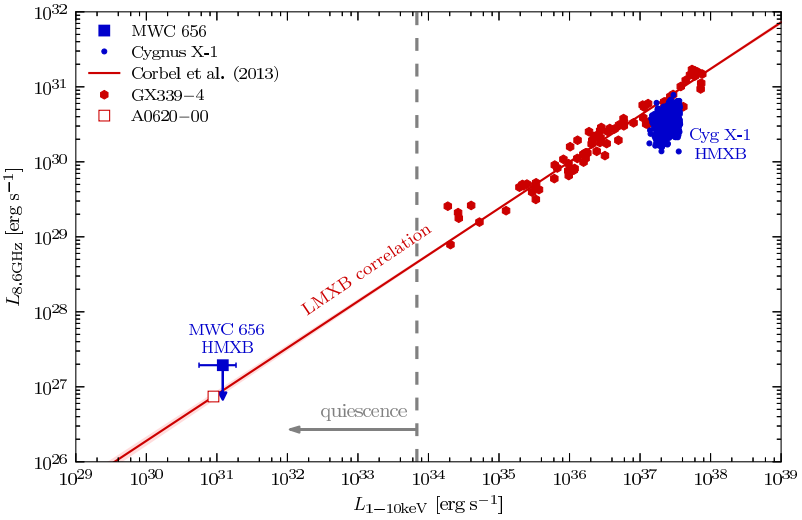

Figure 5: Radio vs X-ray luminosity diagram including the position of MWC 656 (blue square) according to non-simultaneous X-ray observation (accounting only for the non-thermal contribution) and the lowest radio flux density upper limit from Moldón (2012). The small blue dots indicate the region of the parameter space where Cygnus X-1 has been detected in the low/hard state (Gallo et al. 2012). It is also plotted the radio/X-ray correlation for BH LMXBs of Corbel et al. (2013) (red solid line plus light red shadow), together with data on the BH LMXBs GX 339−4 (red hexagons) and A0620−00 (empty red square) to display the luminosity range of real sources. The gray dashed line separates the quiescent state region (left) from the other states (right) according to the threshold set by Plotkin et al. (2013). The position of MWC 656 is very close to the one of the LMXB A0620−00 in quiescence, indicating that the radio/X-ray correlation might also be valid for BH HMXBs down to very low luminosities. Image from Munar-Adrover et al. (2014).

the faintest low-mass X-ray binaries detected. Munar-Adrover et al. (2014) put together the X-ray measurement and radio upper limits from Moldón et al. (2012) to prove that MWC 656 actually could fit within the radio/X-ray luminosity correlation (Corbel et al. 2013). Consequently, the radio/X-ray correlation might also be valid for BH HMXBs. In this context, MWC 656 will allow the study of accretion processes and of accretion/ejection coupling at very low luminosities for BH HMXBs.

3.5.2 Binary pulsars

The only gamma-ray binary of which we know the nature of the compact object is PSR B1259−63, which contains a young non-accreting millisecond pulsar orbiting a O star with a decretion disk every 3.4 years (Negueruela et al. 2011). The orbital plane of the pulsar is inclined with respect to the disk of the companion star. In X-rays this system shows a regular behaviour with two peaks in its light-curve 20 days before and after periastron passage (Chernyakova et al. 2009). This emission is produced well inside the binary system and the variations are consistent with the disk crossing times. In radio the emission can extent up to 10−100 times the binary system size. At gamma rays PSR B1259−63 has been observed in recent times by *Fermi*/LAT and *AGILE* and both have detected a weak source positionally coincident with the binary system. *Fermi*/LAT detected significant flaring emission ∼55 days after periastron passage with a release of energy very close to the spin-down luminosity of the pulsar (Abdo et al. 2011b). Tam et al. (2011) suggested that this was

due to the effect of Doppler boosting in the emission of PSR B1259−63, but very much fine tuning of the models is needed. At VHE PSR B1259−63 has been detected three times by H.E.S.S. when the pulsar was in the vicinity of the periastron passage with similar results in each observation, confirming that the emission is actually coming from the binary system (Aharonian et al. 2005c; H.E.S.S. Collaboration et al. 2013). At phases other than near periastron all VHE observations have yielded upper limits.

A good candidate for the binary pulsar scenario is LS 5039, which is a gamma-ray binary composed by a massive O star and a compact object of unknown nature orbiting the star every ∼3.9 days. This system, proposed to be associated with the *EGRET* source 3EG J1824−1514 (Paredes et al. 2000), has been detected in gamma rays by *Fermi*/LAT (Abdo et al. 2009) and by H.E.S.S. (Aharonian et al. 2005a, 2006e). The minimum flux at VHE is detected near the superior conjunction (or close to periastron) and the maximum occurs at inferior conjunction. At the inferior conjunction a spectral fit with a powerlaw yields $\Gamma_{\rm VHE} \simeq 1.8$ and an exponential cutoff at $E_{\rm c} = 8.7$ TeV. At superior conjunction the source is fainter and can be described with a powerlaw with a softer index $\Gamma \simeq 2.5$. The X-ray flux is also modulated with the orbital period. The emission is enhanced (reduced) when the highly relativistic electrons seen by the observer encounter the seed photons head-on (rear-on), i.e., at superior (inferior) conjunction. The absorption due to pair production will be maximum (minimum) at superior (inferior) conjunction. Zabalza et al. (2013) propose a model to explain the VHE emission in this binary system, within the binary pulsar scenario: they suggest that there are two main VHE emitters, one located at the wind standoff, where the wind of the companion and the wind of the pulsar collide head-on; and the Coriolis turnover, which is produced due to the orbital motion of the binary system and is located at a distance larger than the orbital separation. However the effort in modeling the emission with this approach, the increasing number of observations and their improved quality showcases the difficulty in understanding the processes that produce non-thermal emission in gamma-ray binaries.

4. Conclusions

Gamma-ray astronomy has grown fast in the last decades thanks to the developement of very sensitive instruments, such as the current IACT family and the gamma-ray space telescopes. They have brought new insights to the extreme universe and the processes behind the HE and VHE emission. AGN observations led to the first observational evidences for correlated optical and VHE emission, suggesting that optical photons are the target for the IC process, putting important constraints into emission models. Perhaps one of the most impressive results is the first observational evidence of the acceleration of CR in SNRs, as seen in IC 433 and W44. This confirms the theoretical interpretation proposed decades ago. PWN have demonstrated also that not everything is known. The Crab Nebula showed unprecedented flaring emission in this system, demonstrating that even the standard candles must be studied carefully. It is still not known how these flares are produced and more detailed studies and observations are needed. In the field of binary systems we see an increase in the number of known systems that emit in gamma rays (1FGL J1018.6−5856), and new candidates appear, such as MWC 656, which is also the first Be/BH binary system discovered. The study of known gamma-ray binaries as PSR B1259−63 and LS 5039 allow us to put constraints to the emission models and thanks to new very-good quality data we will be able to

even improve those models in order to explain what our telescopes detect.

Acknowledgements
We acknowledge support by the Spanish Ministerio de Economía y Competitividad (MINECO) under grants AYA2013-47447-C3-1-P, MDM-2014-0369 of ICCUB (Unidad de Excelencia 'María de Maeztu'), and the Catalan DEC grant 2014 SGR 86. J.M.P. acknowledges financial support from ICREA Academia.

References

Abdo, A. A., Ackermann, M., Ajello, M., et al. 2010, ApJ, 714, 927
Abdo, A. A., Ackermann, M., Ajello, M., et al. 2011a, Science, 331, 739
Abdo, A. A., Ackermann, M., Ajello, M., et al. 2011b, ApJL, 736, L11
Abdo, A. A., Ackermann, M., Ajello, M., et al. 2009, ApJL, 706, L56
Acciari, V. A., Aliu, E., Arlen, T., et al. 2011, ApJL, 730, L20
Acciari, V. A., Aliu, E., Arlen, T., et al. 2009a, Science, 325, 444
Acciari, V. A., Aliu, E., Arlen, T., et al. 2009b, ApJL, 698, L94
Ackermann, M., Ajello, M., Allafort, A., et al. 2013, Science, 339, 807
Aharonian, F., Akhperjanian, A. G., Anton, G., et al. 2009, A&A, 503, 817
Aharonian, F., Akhperjanian, A. G., Aye, K.-M., et al. 2005a, Science, 309, 746
Aharonian, F., Akhperjanian, A. G., Aye, K.-M., et al. 2005b, A&A, 435, L17
Aharonian, F., Akhperjanian, A. G., Aye, K.-M., et al. 2005c, A&A, 442, 1
Aharonian, F., Akhperjanian, A. G., Aye, K.-M., et al. 2004, A&A, 425, L13
Aharonian, F., Akhperjanian, A. G., Bazer-Bachi, A. R., et al. 2007a, ApJL, 664, L71
Aharonian, F., Akhperjanian, A. G., Bazer-Bachi, A. R., et al. 2006a, A&A, 449, 223
Aharonian, F., Akhperjanian, A. G., Bazer-Bachi, A. R., et al. 2007b, A&A, 464, 235
Aharonian, F., Akhperjanian, A. G., Bazer-Bachi, A. R., et al. 2006b, Science, 314, 1424
Aharonian, F., Akhperjanian, A. G., Bazer-Bachi, A. R., et al. 2006c, A&A, 460, 365
Aharonian, F., Akhperjanian, A. G., Bazer-Bachi, A. R., et al. 2006d, A&A, 460, 743
Aharonian, F., Akhperjanian, A. G., Bazer-Bachi, A. R., et al. 2006e, A&A, 460, 743
Aharonian, F. A. 2000, Nature, 5, 377
Aharonian, F. A., Akhperjanian, A. G., Bazer-Bachi, A. R., et al. 2005d, A&A, 442, L25
Aharonian, F. A., Bogovalov, S. V., & Khangulyan, D. 2012, Nature, 482, 507
Albert, J., Aliu, E., Anderhub, H., et al. 2008, ApJL, 685, L23
Albert, J., Aliu, E., Anderhub, H., et al. 2009, ApJ, 693, 303
Albert, J., Aliu, E., Anderhub, H., et al. 2006a, ApJL, 638, L101
Albert, J., Aliu, E., Anderhub, H., et al. 2006b, Science, 312, 1771
Albert, J., Aliu, E., Anderhub, H., et al. 2007a, ApJ, 669, 862
Albert, J., Aliu, E., Anderhub, H., et al. 2007b, ApJL, 665, L51
Aleksić, J., Alvarez, E. A., Antonelli, L. A., et al. 2012a, A&A, 541, A13
Aleksić, J., Alvarez, E. A., Antonelli, L. A., et al. 2012b, ApJL, 754, L10
Aleksić, J., Alvarez, E. A., Antonelli, L. A., et al. 2012c, A&A, 540, A69
Aleksić, J., Alvarez, E. A., Antonelli, L. A., et al. 2012d, ApJ, 746, 80
Aliu, E., Anderhub, H., Antonelli, L. A., et al. 2008, Science, 322, 1221
Aliu, E., Archambault, S., Aune, T., et al. 2014, ApJ, 780, 168
Anderhub, H., Antonelli, L. A., Antoranz, P., et al. 2009, ApJL, 706, L27

Araudo, A. T., Bosch-Ramon, V., & Romero, G. E. 2009, A&A, 503, 673
Atoyan, A. M. & Dermer, C. D. 2003, ApJ, 586, 79
Ballantyne, D. R., Schumann, M., & Ford, B. 2011, MNRAS, 410, 1521
Bednarek, W. & Idec, W. 2011, MNRAS, 414, 2229
Bednarek, W. & Sobczak, T. 2014, International Journal of Modern Physics Conference Series, 28, 60171
Bosch-Ramon, V. & Khangulyan, D. 2009, International Journal of Modern Physics D, 18, 347
Bühler, R. & Blandford, R. 2014, Reports on Progress in Physics, 77, 066901
Bulgarelli, A., Pittori, C., Lucarelli, F., et al. 2010, The Astronomer's Telegram, 2512, 1
Casares, J., Negueruela, I., Ribó, M., et al. 2014, Nature, 505, 378
Casares, J., Ribó, M., Ribas, I., et al. 2012, MNRAS, 421, 1103
Cerutti, B., Uzdensky, D. A., & Begelman, M. C. 2012, ApJ, 746, 148
Chernyakova, M., Neronov, A., Aharonian, F., Uchiyama, Y., & Takahashi, T. 2009, MNRAS, 397, 2123
Corbel, S., Coriat, M., Brocksopp, C., et al. 2013, MNRAS, 428, 2500
Cordes, J. M. & Lazio, T. J. W. 2002, ArXiv Astrophysics e-prints
Coroniti, F. V. 1990, ApJ, 349, 538
Crocker, R. M., Jones, D. I., Aharonian, F., et al. 2011, MNRAS, 413, 763
Dubus, G. 2013, A&A Rev, 21, 64
Dubus, G., Cerutti, B., & Henri, G. 2010, MNRAS, 404, L55
Eckart, A., Mužić, K., Yazici, S., et al. 2013, MmSAI, 84, 618
Fermi LAT Collaboration, Abdo, A. A., Ackermann, M., et al. 2009, Science, 326, 1512
Fermi LAT Collaboration, Ackermann, M., Ajello, M., et al. 2012, Science, 335, 189
Gaensler, B. M., Schulz, N. S., Kaspi, V. M., Pivovaroff, M. J., & Becker, W. E. 2003, ApJ, 588, 441
Gallo, E., Miller, B. P., & Fender, R. 2012, MNRAS, 423, 590
Gillessen, S., Genzel, R., Fritz, T. K., et al. 2012, Nature, 481, 51
H. E. S. S. Collaboration, Abramowski, A., Acero, F., et al. 2012, A&A, 541, A5
H.E.S.S. Collaboration, Abramowski, A., Acero, F., et al. 2013, A&A, 551, A94
Hooper, D. & Linden, T. 2011, PhRvD, 84, 123005
Hwang, U., Decourchelle, A., Holt, S. S., & Petre, R. 2002, ApJ, 581, 1101
Katsuda, S., Petre, R., Hughes, J. P., et al. 2010, ApJ, 709, 1387
Lyubarsky, Y. & Kirk, J. G. 2001, ApJ, 547, 437
Lyutikov, M. 2014, Astronomische Nachrichten, 335, 227
Mannheim, K. & Biermann, P. L. 1992, A&A, 253, L21
Maraschi, L., Ghisellini, G., & Celotti, A. 1992, ApJL, 397, L5
Maraschi, L. & Treves, A. 1981, MNRAS, 194, 1P
Marscher, A. P. & Gear, W. K. 1985, ApJ, 298, 114
Mirabal, N. 2013, MNRAS, 436, 2461
Moldón, J. 2012, PhD thesis, Universitat de Barcelona
Moldón, J., Ribó, M., & Paredes, J. M. 2012, A&A, 548, A103
Munar-Adrover, P., Paredes, J. M., Ribó, M., et al. 2014, ApJL, 786, L11
Negueruela, I., Ribó, M., Herrero, A., et al. 2011, ApJL, 732, L11
Neronov, A., Semikoz, D., & Sibiryakov, S. 2008, MNRAS, 391, 949
Paredes, J. M., Bednarek, W., Bordas, P., et al. 2013, Astroparticle Physics, 43, 301
Paredes, J. M., Martí, J., Ribó, M., & Massi, M. 2000, Science, 288, 2340
Pittori, C., Verrecchia, F., Chen, A. W., et al. 2009, A&A, 506, 1563
Plotkin, R. M., Gallo, E., & Jonker, P. G. 2013, ApJ, 773, 59

Rees, M. J. & Gunn, J. E. 1974, MNRAS, 167, 1
Romero, G. E., Del Valle, M. V., & Orellana, M. 2010, A&A, 518, A12
Sabatini, S., Striani, E., Verrecchia, F., et al. 2010, The Astronomer's Telegram, 2715, 1
Tam, P. H. T., Huang, R. H. H., Takata, J., et al. 2011, ApJL, 736, L10
Tavani, M., Bulgarelli, A., Piano, G., et al. 2009, Nature, 462, 620
Tavani, M., Bulgarelli, A., Vittorini, V., et al. 2011, Science, 331, 736
VERITAS Collaboration, Aliu, E., Arlen, T., et al. 2011, Science, 334, 69
Warren, J. S., Hughes, J. P., Badenes, C., et al. 2005, ApJ, 634, 376
Williams, S. J., Gies, D. R., Matson, R. A., et al. 2010, ApJL, 723, L93
Zabalza, V., Bosch-Ramon, V., Aharonian, F., & Khangulyan, D. 2013, A&A, 551, A17